Czech Technical University in Prague

Faculty of Nuclear Sciences and Physical Engineering

RESEARCH WORK

EVALUATION OF THE INNER DETECTOR WITH MUON TRACKS

Bc. Tomáš Jakoubek

Supervisor: Prom. fyz. Václav Vrba, CSc.

September 10, 2009

Acknowledgements

I would like to thank my supervisor Václav Vrba for his invaluable help during creation of this work and for introducing me to CERN and the ATLAS experiment. I am also grateful to the Institute of Physics of the Academy of Sciences of the Czech Republic, mainly to my colleagues Michal Marčišovský and Pavel Růžička for their valuable advice and to Jiří Popule for the material and organizational support during my whole work. Last but not least, I would like to thank my family and friends, especially to Tereza Liepoldová, for their support up until now.

Declaration

I declare that I wrote my research work independently and exclusively with the use of cited bibliography.

I agree with the usage of this thesis in the purport of the Act 121/2000 (Copyright Act).

Prague, September 10, 2009 Tomáš Jakoubek

Title: **Evaluation of the Inner Detector with Muon Tracks**

Author: Bc. Tomáš Jakoubek

Field of study: Nuclear Engineering

Specialization: Experimental Nuclear Physics

Sort of project: Research Work

Supervisor: Prom. fyz. Václav Vrba, CSc. Department of Physics, Faculty of Nuclear Sciences and Physical Engineering, Czech Technical University in Prague

Abstract: Nowadays the ATLAS detector is assembled underground and is ready to take real data. However, separate parts of the detector had not been tested together before. Thus we need to align them to prevent wrong interpretation of the detector output. This research work is dedicated to using cosmic muons for evaluation of the ATLAS tracking system. For this purpose the combined run 91890 was used. First of all, three agreed sets of cosmic cuts are compared in terms of distributions of track parameters and numbers of particles passing through. Next part shows differences between Inner Detector and Muon Spectrometer track reconstruction and thus the alignment between these parts of the ATLAS detector. Comparisons between real and simulated data are shown. Finally some cosmic ray studies are presented.

Keywords: ATLAS, Inner Detector, cosmic muons, evaluation, alignment.

Contents

Chapter 1

Short Overview of Particle Physics

For last forty years the Standard Model is the best theory describing particles and their interactions. This model postulates that there are twelve elementary particles which form all known matter in our universe. These particles are fermions (have half-integral spin) and can be divided into three families (see Tab. 1.1). In each family there are two leptons and two quarks. At present there is no explanation for this triple repetition of fermion families.

The fundamental fermions interact via all known interactions, however the gravitational interaction has not yet been included into the Standard Model. Electromagnetic interaction is mediated by massless photon and has $U(1)$ symmetry, weak interaction is mediated by very massive $W^{\pm}$ and Z^0 bosons and the symmetry is $SU(2)$. Strong interaction is described by Quantum Chromodynamics, which is based on $SU(3)$ symmetry and assigns "colours" to quarks and gluons. Therefore, the internal symmetry of the Standard Model is $SU(3) \times SU(2) \times U(1)$.

	Q [e]	1st generation		2nd generation		3rd generation	
Leptons	-1	e	electron	μ	muon	τ	tauon
	0	ν_e	electron neutrino	ν_μ	muon neutrino	ν_τ	tau neutrino
Quarks	$+\frac{2}{3}$	u	up	c	charm	t	top
	$-\frac{1}{3}$	d	down	s	strange	b	bottom

Table 1.1: Three families of fundamental fermions. The families (generations) are structured according to increasing mass (the first generation is the lightest).

Since 1970s, when the theory was formulated, it passed all experimental tests and all predicted particles have been found except the Higgs boson (all SM particles are summarized in Tab. 1.2 and Tab. 1.3). Higgs boson is the quantum of the theoretical Higgs field. In today's version of the electroweak theory, the $W^{\pm}$ and Z^0 bosons and all the fundamental fermions (quarks and leptons) get their masses by interacting with this field. More they interact, the heavier they become, whereas particles that never interact are left with no mass at all.

Quark	m [GeV/c^2]	Lepton	m [MeV/c^2]
d	$(3.0 \div 7.0) \times 10^{-3}$	e	0.511
u	$(1.5 \div 3.0) \times 10^{-3}$	ν_e	$< 2.3 \times 10^{-6}$
s	$(95 \pm 25) \times 10^{-3}$	μ	105.658
c	1.25 ± 0.09	ν_μ	< 0.17
b	4.20 ± 0.07	τ	1776.99
t	174.2 ± 3.3	ν_τ	< 18.2

Table 1.2: Fundamental fermions and their masses. Data are taken from [1].

	Particle	Spin [$\hbar$]	Q[|e|]	m [GeV/c^2]
EM interaction	photon γ	1	0	0
Weak interaction	$W^{\pm}$	1	± 1	80.398
	Z^0	1	0	91.1876
Strong interaction	gluons g	1	0	0
Higgs field	H (?)	0	0	> 114.4

Table 1.3: Basic properties of Standard Model bosons. The Higgs particle (or particles) has not yet been observed. Data are taken from [1].

Since the Higgs boson is so crucial in Standard Model, much of today's research in high energy physics focuses on the search for this particle. Unfortunately, the Standard Model does not predict its mass. The lower limit is 114.4 GeV, which is the combined result from four **L**arge **E**lectron-**P**ositron Collider (LEP) experiments. Fig. 1.1 shows this in terms of the confidence level as a function of the Higgs mass. However, the LEP collaboration was unable to see any Higgs signal. The same situation seems to be at Tevatron, the current[1] largest particle accelerator, although its energy is 1.96 TeV.

[1]June 2009

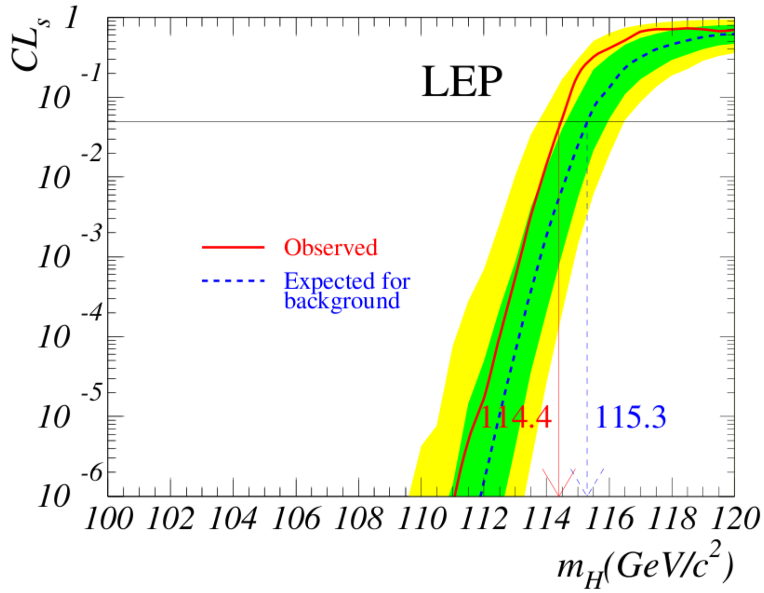

Figure 1.1: The lower limit of a Higgs mass from four-experiment combined result of the LEP Standard Model Higgs search. The figure shows the confidence level CL_s as a function of the Higgs mass. The green and yellow bands around the median expected line correspond to the 1 and 2σ probability bands computed with a large number of simulated background experiments. The intersection of the horizontal line at $CL_s = 0.05$ with the observed curve defines the 95% confidence level lower limit for the mass of the Higgs boson (114.4 GeV). Figure from [2].

To detect the Higgs boson is one of the main goals of the **L**arge **H**adron **C**ollider (LHC), which will be launched again this year[2]. This accelerator is designed for the center of mass energy of 14 TeV in *pp* collisions. Due to the large energy, the LHC should be a Higgs factory, if in fact exists. The cross section of main Higgs production channels at the LHC as a function of the Higgs mass is shown on the Fig. 1.2. As shown, the dominant channel will be the gluon fusion, other processes will be at least one order of magnitude smaller. For experimentalists however, Higgs *decay channels* are probably more interesting than used *production channel*, because the decay products are the only ones we could see. The branching ratios of various decay channels are shown on the Fig. 1.3, but some of them would not be identifiable against the background. The W^+W^- channel seems to be the most promising for heavier Higgs, for lighter Higgs that is the $\tau^+\tau^-$ channel. The $b\bar{b}$ channel is not so amazing as it looks like because of the pure QCD processes $t\bar{t} \to b\bar{b}$ and $t\bar{t} \to jj$ background [2].

[2] 2009

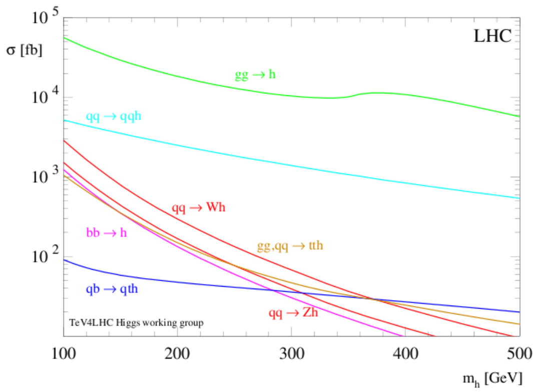

Figure 1.2: Cross sections for Higgs production in various channels at LHC. Figure from [2].

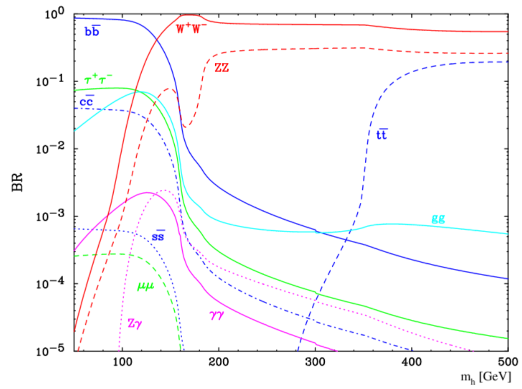

Figure 1.3: Select Standard Model Higgs boson branching ratios as a function of the Higgs mass. The Higgs prefers to decay to the most massive possible final state. Note the *log* scale. Figure from [2].

Some scientists believe that our inability to predict the Higgs mass is a result of the fact that the Standard Model cannot tell the whole story. They are searching for extensions to the electroweak theory that make it more predictive. One approach is a generalization of this theory, called supersymmetry. It postulates a fermion-boson symmetry, according to which new fermion (boson) partners are postulated for all known fundamental bosons (fermions). These superpartners should be heavier than the known elementary particles, but the accurate predictions of the the superpartner masses do not exist. However, there are some distinct arguments that make qualitative predictions of the masses - a typical superpartner mass should be in the range of $100 \div 1000$ GeV [3], [4], which falls in the LHC energy range. This accelerator will be briefly described in the next chapter, the major part will be then devoted to the ATLAS experiment, one of the general-purpose LHC detectors (and the one I am participating on).

Chapter 2

The ATLAS experiment

The world's most powerful accelerator, the **L**arge **H**adron **C**ollider (LHC), was finished at CERN last year. This year[1], after a small break, it will be launched again. The LHC is a synchrotron designed for *pp* collisions with the center of mass energy of 14 TeV and also heavy ions (nuclei of lead, Pb^{82+}) collisions with energy of 1150 TeV. In addition to the greatest energy, the LHC also aims for the greatest luminosity. That should reach 10^{34} $\text{cm}^{-2} \cdot \text{s}^{-1}$ and 100 fb^{-1} of the integrated luminosity per year. To achieve these values, the beams have to have the corresponding density - in each beam there will be 2808 bunches of 1.15×10^{11} particles. Bunches will be separated by 25 ns, thus the bunch crossing rate will be 40 MHz. Another interesting fact is the pressure in the beampipes (10^{-13} atm) and the magnetic field (about 8.33 T) produced by superconducting magnets, which will be cooled to remarkable temperature of 1.9 K. For more information see [6].

To measure the outcome of this powerful accelerator, there are four major and some smaller experiments along the course of the LHC ring (locations of major experiments are on the Fig. 2.1):

ATLAS (**A** **T**oroidal **L**HC **A**pparatu**S**) is a general-purpose detector designed to cover the widest possible range of physics at the LHC. The main goals of the ATLAS experiment are the search for the Higgs boson, the study of CP-violation, the precise measurement of mass of heavy particles, the search for appropriate superparticles or extra dimensions and for particles that could make up *dark matter* - a (still hypothetical) form of matter that does not emit or reflect enough electromagnetic radiation to be observed directly, but whose

[1] 2009

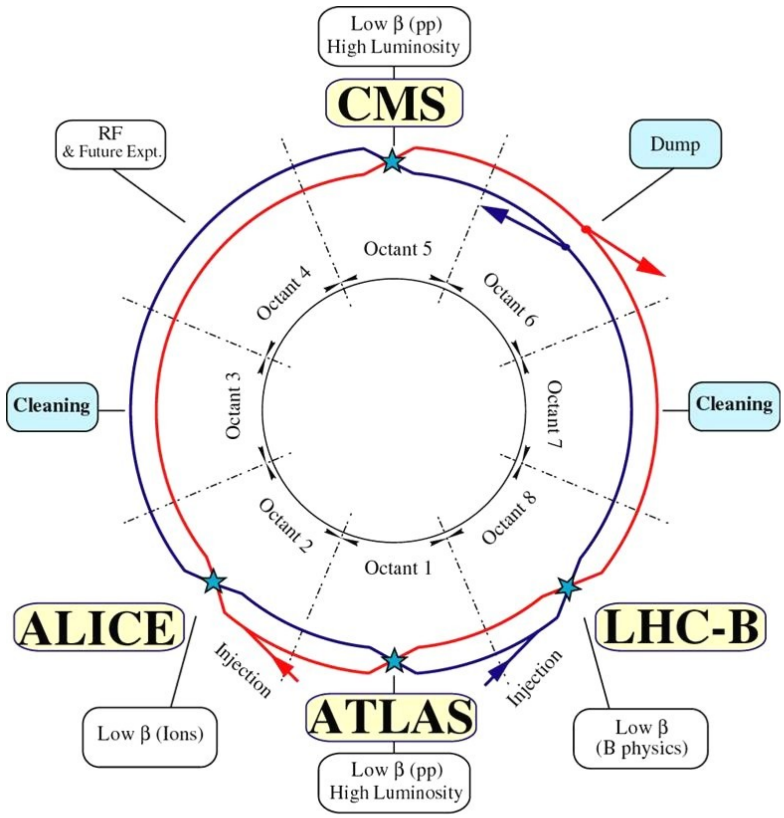

Figure 2.1: The scheme of the LHC and locations of four major experiments. Two smaller experiments are placed near ATLAS (LHCf) and CMS (TOTEM). Figure from [5].

presence can be inferred from gravitational effects. ATLAS is the largest collider detector ever constructed. Its parts will be described in following sections.

CMS (**C**ompact **M**uon **S**olenoid) is also a general-purpose detector, optimized for tracking muons. The word "compact" means that is smaller than the ATLAS detector. CMS and ATLAS have the same physics goals, but different technical solutions and design. That means they can independently confirm the results flowing from the same physical phenomena and reduce systematic and random errors. Moreover, CMS will also try to study heavy ion collisions and the *QGP*.

ALICE (**A** **L**arge **I**on **C**ollider **E**xperiment) is a detector specialized in analysing heavy ions collisions and it will study the properties of quark-gluon plasma.

LHCb (**L**arge **H**adron **C**ollider **b**eauty) specializes in the study of the slight asymmetry between matter and antimatter present in interactions of B-particles and thus help us to understand why the Universe we live in appears to be composed almost entirely of matter, but no antimatter.

LHCf (**L**arge **H**adron **C**ollider **f**orward) is a small experiment designed for astroparticle physics. It will measure particles produced very close to the direction of the beams in the *pp* collisions. The motivation is to test models used to estimate the primary energy of the ultra high-energy cosmic rays.

TOTEM (**TOT**al **E**lastic and diffractive cross section **M**easurement) will measure the effective size or "cross-section" of the proton at LHC, study forward particles to focus on physics that is not accessible to the general-purpose experiments and also independently monitor the luminosity of the LHC.

As mentioned above, ATLAS has really ambitious goals, so it has to be very complex, has high resolution tracking and precise energy measurements. The detector consists of four major components: the *Inner Detector* which measures tracks of all charged particles, the *calorimeter* which measures the energies carried by the particles, the *muon spectrometer* which identifies and measures muons and the *magnet system*. Some of them will be described below. The schematic view of the whole detector with all mentioned components is on the Fig. 2.2.

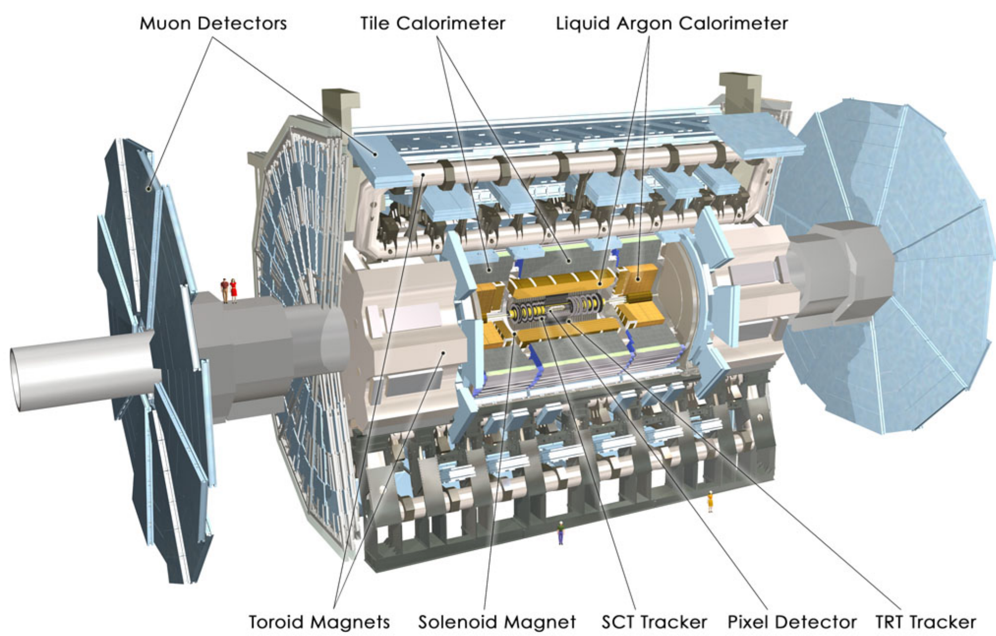

Figure 2.2: The schematic view of the ATLAS detector. Figure from [7].

2.1 ATLAS Coordinate System

The ATLAS Coordinate System is a right-handed system with the x-axis pointing to the centre of the LHC ring, the z-axis following the beam direction and the y-axis going upwards. In Point 1, positive z points towards Point 8.

The azimuthal angle $\phi = 0$ corresponds to the positive x-axis and ϕ increases clock-wise looking into the positive z direction. ϕ is measured in the range $\langle -\pi, +\pi)$. The polar angle θ is measured from the positive z axis. Pseudorapidity η is defined by

$$\eta = -\log\left(\tan\frac{\theta}{2}\right) \tag{2.1}$$

Transverse momentum p_T is the momentum perpendicular to the LHC beam axis. Transverse impact parameter d_0 is defined as the distance of the closest approach of helix to beampipe and longitudinal impact parameter z_0 as the z value at the point of closest approach. The convention for the sign of d_0 is the following: may ϕ denote the azimuthal angle to the perigee position and ϕ_0 the azimuthal angle of the momentum in the perigee. The sign of d_0 is then defined as positive, if $\phi - \phi_0 = \frac{\pi}{2} + n \cdot 2 \cdot \pi$, where $n \in Z_0$. Fig. 2.3 shows these parameters, split into transverse parameters (x-y plane) and longitudinal parameters (r-z view).

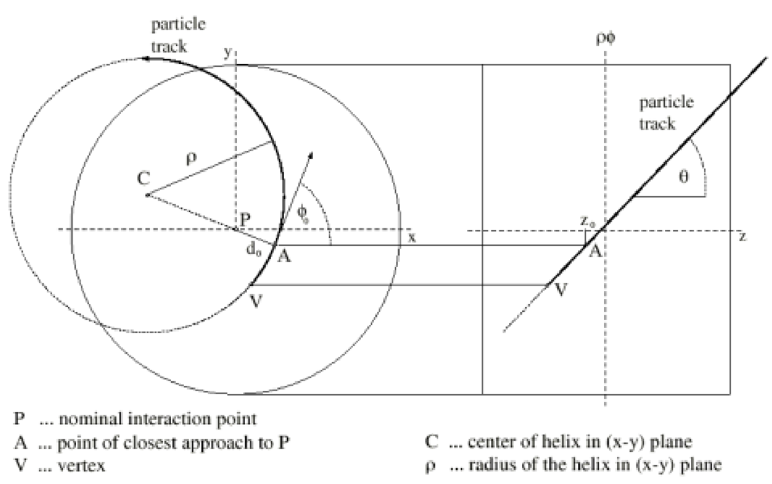

Figure 2.3: The drawing of main track parameters used in the ATLAS detector. Figure from [16].

2.2 Tracking System

Precise ATLAS tracking is done by the Inner Detector, which combines high-resolution detectors at the inner part with continuous straws of Transition Radiation Tracker (see below) at the outer part, all contained in the central solenoid which provides a nominal magnetic field of 2 T. The outer radius is 1.15 m and the total length is 7 m. The Inner Detector should give us detailed tracking information about the first part of the particle's trajectory - it covers a pseudorapidity range up to $|\eta| < 2.5$. The momentum and vertex resolution requirements from physics call for high-precision measurements to be made with fine-granularity detectors, given the very large track density. Semiconductor tracking detectors, using pixel and silicon microstrip technologies offer these features. As shown on the Fig. 2.4, the Inner Detector consists of three subsystems which will be described below. All relevant dimensions are shown on the Fig. 2.5.

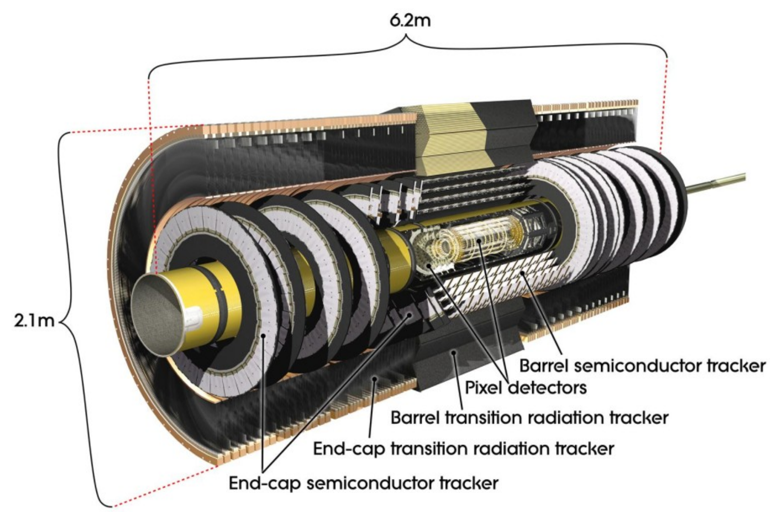

Figure 2.4: The schematic view of the ATLAS Inner Detector. Figure from [7].

2.2.1 Pixel Detector

The Pixel detector is the innermost part of the Inner Detector. It provides a very high-granularity, high-precision set of measurements as close to the interaction point as possible. The system determines the impact parameter resolution and the ability of the Inner Detector to find short-lived particles such as B hadrons and τ leptons.

The detector consists of three barrels and three disks of each endcap. The barrel layers are made of identical staves inclined with azimuthal angle of 20° and each stave is composed of 13 pixel modules (or so-called "wafers"). One endcap disk is made of 8 sectors, with 6 modules in each sector (disk modules are identical to the barrel modules, except the connecting cables). All in all there are 1744 pixel modules.

The wafer dimensions are 16.4 mm × 60.8 mm and on each there are 16 front-end chips and one module control chip. One front-end chip contains 16 columns of 400 μm and 2 columns of 600 μm (so-called *long*) pixels, and 160 normal plus 4 ganged rows of 50 μm pixels. Thus, the short side of the module has a 50 μm pitch and the long side has a 400 μm pitch with the only exception of long and ganged pixels. The intrinsic accuracies in the barrel are 10 μm (R-ϕ) and 115 μm (z) and in the disks are 10 μm (R-ϕ) and 115 μm (R). The Pixel detector has approximately 80.4 million readout channels.

2.2.2 Semiconductor Tracker

The second part of the Inner Detector is the **S**emi**C**onductor **T**racker (SCT). Its design is very similarly to the Pixel detector, but instead of pixels it uses the silicon strips for detection. This system will provide eight precision measurements per track in the intermediate radial range, contributing to the measurement of momentum, impact parameter and vertex position.

The barrel part of the detector uses eight layers of silicon microstrip sensors to provide precision position measurement. The modules are mounted on carbon-fibre cylinders which carry the cooling system. The endcap modules are mounted in up to three rings onto nine wheels, which are interconnected by a space-frame. Each silicon sensor is 6.36 cm × 6.40 cm with 768 readout strips of 80 μm pitch. The intrinsic accuracies per module in the barrel are 17 μm (R-ϕ) and 580 μm (z) and in the disks are 17 μm (R-ϕ) and 580 μm (R). The total number of readout channels in the SCT is approximately 6.3 million.

2.2.3 Transition Radiation Tracker

The last part of the Inner Detector is the **T**ransition **R**adiation **T**racker (TRT), which covers a pseudorapidity range up to $|\eta| < 2.0$. It is based on the use of straw detectors, which can operate at the expected high rates due to their small diameter. This system detects the transition radiation photons which were created by passing particles.

The barrel contains about 50 000 straws, each divided in two at the center, and the endcaps contain 320 000 radial straws. Each straw is 4 mm in diameter and equipped with a 30 μm diameter gold-plated wire. Because of a large number of the straws, TRT produces about 30 hits for each track.

The TRT only provides R-ϕ information, for which it has an intrinsic accuracy of 130 μm per straw. In the barrel region, the straws are parallel to the beam axis and are 144 cm long, with their wires divided into two halves, approximately at $\eta = 0$. In the end-cap region, the 37 cm long straws are arranged radially in wheels. The total number of TRT readout channels is approximately 351,000.

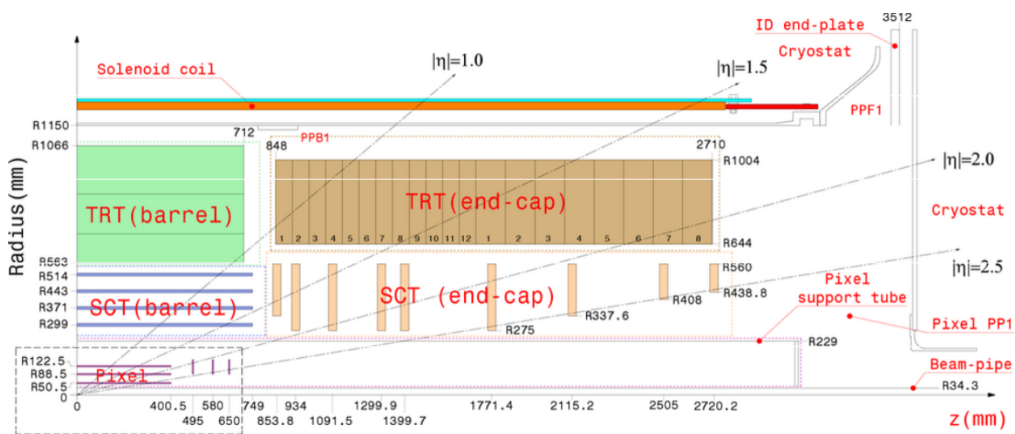

Figure 2.5: The plan view of a quarter-section of the ATLAS Inner Detector showing each of the major elements with its active dimensions. Figure from [12].

2.3 Muon Detection

The only charged particles that can travel through all of the calorimeter material placed around the Inner Detector are muons. They lose energy almost entirely by the formation of electron-ion pairs along their path, and for a substance like steel, this amounts to an energy loss of about 1.57 MeV per millimetre of path. Thus muons with energy above 5 GeV will penetrate about 7.8 m of steel, whereas hadrons of almost any energy are completely absorbed in about 2 m of steel. Thus it is nearly certain that energetic particles seen outside the hadron calorimeter are muons.

The Muon Spectrometer covers the pseudorapidity range $|\eta| < 2.7$ and allows identification of muons with momentum above 3 GeV/c and precise determination of p_T up to about 1 TeV/c. To measure it, superconducting coils (see Fig. 2.6) provide a toroidal magnetic field whose integral varies significantly as a function of both η and ϕ. The integrated bending strength is roughly constant as a function of η except for a significant drop in the transition between the barrel and endcap toroid coils ($1.4 \lesssim |\eta| \lesssim 1.6$).

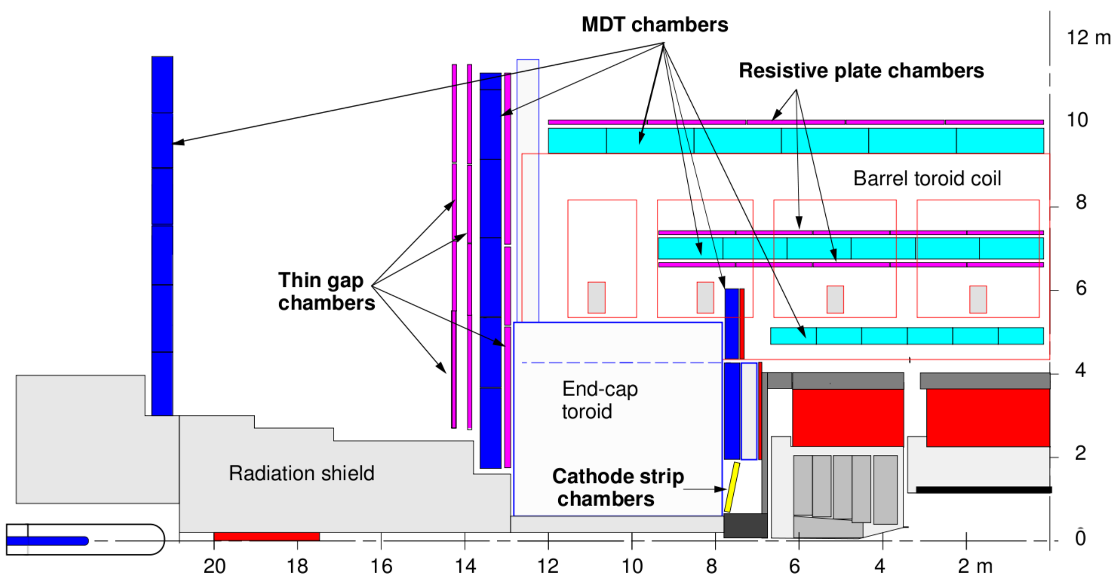

Figure 2.6: The plan view of a quarter-section of the ATLAS Muon System showing each of the major elements with its active dimensions. Figure from [14].

In the barrel region ($|\eta| < 1$), muons are measured in three widely-separated layers of chambers consisting of precise **M**onitored **D**rift **T**ubes (MDTs) and fast **R**esistive **P**late **C**hambers (RPCs) used for triggering. MDTs stations includes multiple closely-packed layers measuring the η coordinate (the direction in which most of the magnetic field deflection occurs) and provide these measurements everywhere except in the high η region ($|\eta| > 2.0$, the endcap regions) of the innermost station. There **C**athode **S**trip **C**hambers (CSCs) are used for precise measuring and **T**hin **G**ap **C**hambers (TGCs) for triggering. The MDTs measurement precision in each layer is typically better than 100 μm, the CSCs additionally provide a rough (1 cm) measurement of the ϕ coordinate.

2.4 Trigger System

The main task of the ATLAS trigger is not easy: it has to reduce a flux of information from 10^9 Hz to 200 Hz, but it must not to discard interesting events (for example, a Standard Model Higgs particle with a mass of 120 MeV, decaying into two photons, is expected to occur at a rate of 10^{-13} of the interaction rate... the proverbial pin in the haystack).

The triggering process is divided into three steps. The first step (LVL1 trigger) is implemented as a hardware trigger, the second and third steps (LVL2 trigger and Event Filter) are software triggers and are usually referred to as the ATLAS **H**igh **L**evel **T**rigger (HLT). The scheme of the ATLAS trigger is shown on the Fig. 2.7.

LVL1 trigger reduces the initial 40 MHz to less than 75 kHz in less than 2.5 μs. It looks for regions of potentially interesting activity in the Calorimeters and the Muon Spectrometer (RPC for $|\eta| < 1$ and TGC for $1 < |\eta| < 2.4$) that may correspond to candidates for high p_T leptons, hadrons or jets. This is known as **R**egion **o**f **I**nterest (RoI) concept (see Fig. 2.8).

The LVL2 selection is largely based on RoI information of the LVL1 trigger and uses fine-grained data from the detector for a local analysis of the LVL1 candidate. The LVL2 trigger reduces the rate to approx. 1 kHz and its latency is about 10 ms.

Event Filter further reduces the rate to frequency of about 200 Hz (latency is approx. 1 s). The RAW data of the full event are passed to the Event Builder, which collects the pieces of information connected to this event and put them into a single memory. The size of each event saved at the permanent data storage is about 1.5 MB.

A relatively new concept for ATLAS cosmic triggering is so-called *TRT Fast-OR Trigger*. It utilizes a fast trigger generation circuit on the TRT front-end chips (DTMROCs) and a simple trigger logic on the TRT trigger, timing and control board. Other cosmic triggers (such as RPC and TGC) have low track purity, in the barrel and especially in the endcap region. Data from the June 2009 combined run with the full Inner Detector shows a total TRT barrel trigger rate of 8 Hz on cosmic tracks with a track purity from offline reconstruction of 98 %. Using tracks triggered by the RPC detector, the track efficiency in the barrel is estimated to 88 %. The TRT Fast-OR Trigger is well described in [11].

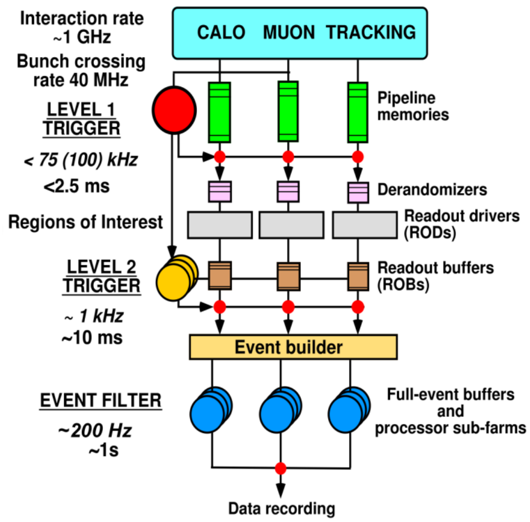

Figure 2.7: The scheme of the ATLAS trigger. Figure from [17].

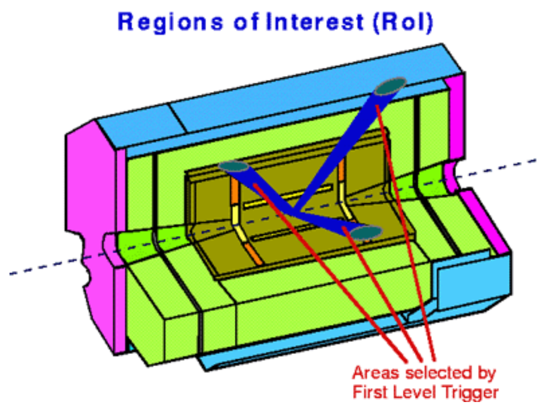

Figure 2.8: The example of Regions of interest selected by LVL1 trigger. These are used by the further trigger levels. Figure from [7].

2.5 ATHENA Framework

There is a need for a common framework for physicists plug-in their ideas. In the case of the ATLAS experiment, that framework is called **Athena**. Athena is based on C++ and Python and it is an enhanced version of the Gaudi framework that was originally developed by the LHCb experiment, but now it is a common ATLAS–LHCb project. Athena and Gaudi are concrete realizations of a component-based architecture (also called Gaudi) which was designed for a wide range of physics data-processing applications. Apart from common data types, methods and functions, Athena also contains a central software repository for all algorithms. Everything can be managed by using the **C**onfiguration **M**anagement **T**ool (CMT). The Athena documentation is based on TWiki [19]; one can found there many manuals, tutorials and user experiences.

Athena uses a unified hierarchy of data types. Each of them has some advantages and disadvantages (mainly the size) [20]:

RAW data are events as output by the Event Filter (see section 2.4) for reconstruction. They can be also used for trigger analysis. The event size should be about 1.6 MB, arriving at an output rate of 200 Hz.

ESD (**E**vent **S**ummary **D**ata) refers to event data written as the output of the reconstruction process. Its content is intended to make access to RAW data unnecessary for most physics applications other than for some calibration or re-reconstruction. ESD has an object-oriented representation, and is stored in POOL ROOT files. The size of an event is about 500 kB

AOD (**A**nalysis **O**bject **D**ata) is a reduced event representation, derived from ESD, suitable for analysis. It contains physics objects and other elements of analysis interest. As ESD, AOD has also an object-oriented representation, and is stored in POOL ROOT files. The target size is 150 kB per event.

TAG data are event-level metadata - thumbnail information about events to support efficient identification and selection of events of interest to a given analysis. The assumed average size is 1 kB per event.

DPD (**D**erived **P**hysics **D**ata) is an n-tuple-style representation of event data for end-user analysis and histogramming. In general people in different groups make different DPD files using the same input data.

It is good to mention that simulated data are often larger, in part because they usually retain Monte Carlo "truth" information.

However, Athena is not only the reconstruction and analysis algorithms for the ATLAS data. It contains also all other software needed for the HEP computing. All these software together form a software chain which is needed to produce the AOD file on which analysis can be performed.

Generation Generators create an output of some physical process - for some initial conditions we get a list of outgoing particles, their position and momentum, with the theoretically predicted probability. For this job, some Monte Carlo (MC) generator is used. Generator quality is highly dependent on our knowledge of the underlying physics. Athena includes many generators, typical examples are Pythia and Herwig (both are written in FORTRAN, not in C++).

Simulation A simulator takes a Lorentz 4-vector of a particle (created by the generator), the detector geometry and its composition. As an output we get a collection of hits, which may carry information like position, energy deposit, identifier of the active element etc. In the Athena framework there are two types of simulation programmes:

G4ATLAS is based on the Geant4 simulation package [21], which provides both the framework and the necessary functionality for running detector simulation. These functionalities include optimized solutions for geometry description, the propagation of particles through detectors, the description of materials, the modelling of physics processes and many more.

Atlfast is a fast simulation programme, which replaces the full detector simulation and reconstruction phases. Fast simulation is performed by smearing the MC truth information directly with resolutions measured in full simulation studies. The speed depends on many factors, but in general it is about 4 orders of magnitude faster than running the full chain.

Digitization In this step, the software takes the hits from simulation and turns them into *what-we-get-from-real-detector*. The algorithm has to take into the account the response of the readout electronics and the imperfection of the detectors like finite resolution, noise or defects. The output files of the digitisation step are called **R**aw **D**ata **O**bjects (RDOs) and should resemble the real data from the detector (and thus these two could be compared).

Reconstruction The main task of the reconstruction is to derive from the stored RAW data (whether real data or MC simulation) specific particle parameters and auxiliary information necessary for physics analysis. That means to find hits, try to fit a track through them and save it together with vertices, jets, missing energy etc. Information from all detectors is combined - common tools are shared between tracking detectors on one side and calorimeters on the other side. The output is stored in ESD and AOD formats (see above).

Analysis In this phase, we have real or simulated data (for example in AOD files) and now we need physicists with their intuition. They should interpret the reconstruction results (for example compute invariant mass of the muon pair in the $Z \to \mu\mu$ events) and try to find what actually happened. For this purpose, every physicist can write his analysis algorithm. In such algorithm, one can use some of various Athena packages (provided by CMT, see [19] for more information) or write a new one on is own. The output of this analysis part can be then visualized in some software - pictures are more comprehensible for human mind than numbers. In the case of the ATLAS experiment there are two ways to do this:

The first one is to plot a histogram. The most used programme is **ROOT**, which is very popular in HEP community. It is an object-oriented framework and is also written in C++. Both frameworks, ROOT and Athena, are well connected, but in general, they are independent. ROOT can be used in an interactive mode (writing the C++ statements on the CINT command line) or it is possible to write a script and then execute it. It is very powerful and universal software, which can be used for example for histogramming and graphing to visualize and analyze distributions and functions, curve fitting (regression analysis) and minimization of residuals, statistics and data analysis, matrix algebra, but also for drawing the Feynman diagrams or 3D visualization of the detector. Many examples, documentation and downloadable binaries/source codes can be found on the ROOT website [22].

The second way is to use an event viewer. In the case of ATLAS, there are two possibilities: **Atlantis** and **VP1** (**V**irtual **P**oint **1**). Both can be used for the visual investigation and the understanding of the physics of complete events, or as a tool for creating pictures and animations for publications and presentations. Atlantis is a stand-alone Java application, which uses simplified detector geometry and provides 2D pictures of some specific event. As an input, it uses so-called *jiveXML* files that have to be produced during reconstruction or analysis on top of the standard output. On the other hand, VP1 runs out of the Athena framework and thus provides direct access to the same data and algorithms. Another advantage of VP1 is e.g. 3D view with direct mouse/keyboard rotation. More information and documentation can be found on the websites [23] and [24].

Chapter 3

Detector Evaluation with Muon Tracks

Cosmic rays were discovered nearly a hundred years ago. Since then they have been studied in detail and also were used as a source of new particles at the beginning of high energy physics. Now, at the time of powerful accelerators, they give us a chance of choice - we can use them to test our detectors. In the case of ATLAS, it is a considerable advantage, because separate parts of the detector had not been tested together before the whole ATLAS detector was assembled underground.

3.1 Cosmic Muons

Every second the Earth atmosphere is bombarded with high-energy particles coming from all directions from outer space. They are produced in events such as supernovas or the formation of black holes, during which they can be accelerated to enormous energies. The observed energy spectrum is very wide, ranging from 10^9 eV to over 10^{20} eV (see Fig. 3.1).

Incoming cosmic rays are mostly protons (almost 90 %), others are alpha particles (about 9 %) and electrons (about 1 %). The remaining fraction is made up of the other heavier nuclei (with an atomic number between 2 and 92). Incoming particles collide with molecules of air in the Earth atmosphere. In this process mostly pions and kaons are created and they further decay to photons, electrons, muons and neutrinos. Particles in this *cosmic ray shower* can interact with molecules of air again. An example of this shower is shown on the Fig. 3.2.

We are interested in cosmic muons, because they are prevalent charged particles at sea level. They are produced typically about 15 km above the ground and lose about 2 GeV to ionization before reaching it. The mean energy of muons at the ground is approx. 4 GeV. Their distribution is $\propto \cos^2\theta$ of the incidence angle and is symmetric in φ. The integral intensity of vertical muons above 1 GeV/c at sea level is approx. 70 $\mathrm{m}^{-2} \cdot \mathrm{s}^{-1} \cdot \mathrm{sr}^{-1}$, which is frequently presented in the form $I \approx 1\ \mathrm{cm}^{-2} \cdot \mathrm{min}^{-1}$ for horizontal detectors. The brief summary of cosmic ray properties can be found in [1]

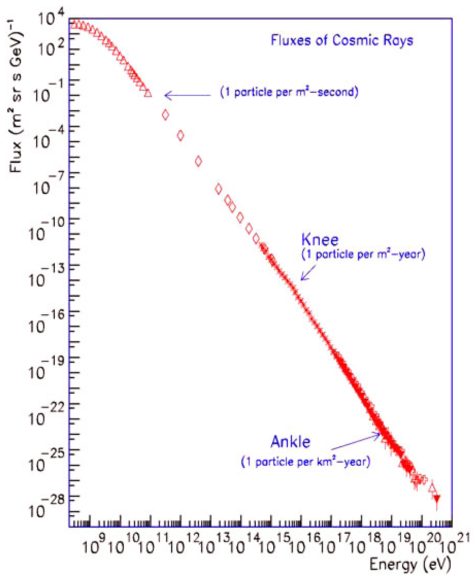

Figure 3.1: The energy spectrum for cosmic rays. The flux of cosmic rays appears to follow a single power law $\sim E^{-3}$ over the range from 10^9 eV to 10^{20} eV. Figure from [9].

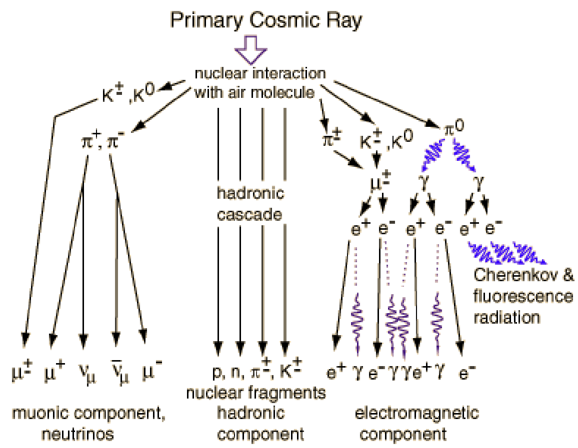

Figure 3.2: The diagram of a cosmic ray shower. It contains hadronic, electromagnetic and muon components (with neutrinos). Figure from [8].

3.2 ATLAS Cosmic Data

Since ATLAS was completed, it has been able to detect cosmic particles (that have enough energy to pass through all the material above the ATLAS cavern). During this period, ATLAS has collected hundreds of millions cosmic events, millions of them have tracks in the Inner Detector. Events have been recorded in separate *runs* with specific options (solenoid/toroid magnetic field on/off, standalone detectors or combined runs and so on). Number of cosmic tracks in the Inner Detector in the year 2008 is shown on the Fig. 3.3.

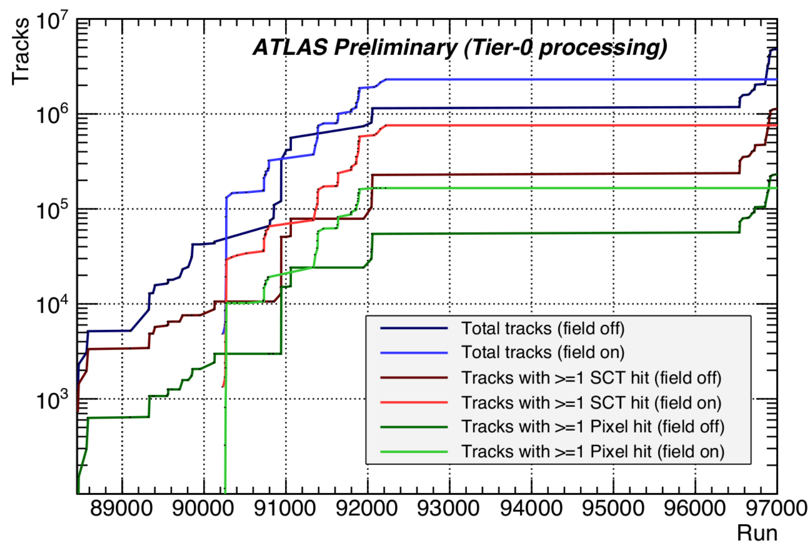

Figure 3.3: Number of cosmic tracks in the Inner Detector in the year 2008. Note the rapid increase after run 96500 caused by *TRT Fast-OR Trigger* (see section 2.4). Figure from [18].

For my research I wanted a combined run with *complete* Inner Detector (ID) and both magnetic fields *ON* and relatively high statistics. Sometimes it is really complicated to find a useful valid dataset, so finally I have chosen the run **91890** that best satisfies all my requirements.

The first part of my research consist in rewriting the Athena package

`PhysicsAnalysis/AnalysisCommon/UserAnalysis`

One can find all modified files (`AnalysisSkeleton.cxx`, `AnalysisSkeleton.h`, `jobOptions.py`, `requirements`, `filelist.py`) in my public directory on AFS (accessible for example from LXPLUS)

`/afs/cern.ch/user/j/jakoubek/public/rework/`

This algorithm, in short, collects suitable cosmic muons from three different collections:

`TrackParticleCandidate`	-	for tracking studies
`StacoMuonCollection`	}	for combined studies
`MuidMuonCollection`		

and save them into trees in a ROOT file (two `MuonCollection` were used because of their comparison; finally I have chosen the `StacoMuonCollection`). These steps have been done twice - for real data (run 91890) and for simulated data:

```
valid2.108867.CosSimIDVolSolOnTorOn.recon.AOD.s533_d167_r676
```

Muon Spectrometer (MS) track parameters are extrapolated to the beam axis and then the track parameters at perigee are compared between MS and ID standalone reconstructions. Combined studies were done with no global ID-MS alignment corrections. The whole analysis has been done with the Athena release 15.2.0.

For analysis of produced files, I have written a ROOT macro (`Comp.C`, it can be also found in my public directory on AFS), which makes all further presented plots and histograms. It can be just executed with "`.x Comp.C`" or loaded first (`.L Comp.C`) and then run with arguments

```
Comp(RD_file,MC_file,IMG_save,Collection)
```

where

`RD_file (char)`	ROOT file with real data, default: `"rd.root"`
`MC_file (char)`	ROOT file with simulated data, default: `"mc.root"`
`IMG_save (int)`	`0` - just plot histograms, `1` - save them as `PNG`, default: `0`
`Collection (char)`	can be `"STACO"` or `"MUID"`, default: `"STACO"`

3.3 Analysis Results

The first thing I was interested in was the Inner Detector tracking. As you can see on the Fig. 3.4, at least one silicon hit is necessary for a good track fitting. With no silicon hit, algorithm uses only TRT and thus practically all information about z_0 and η are lost (see the TRT design in section 2.2.3). That is one of reasons why ID group has suggested three sets of cuts for cosmic tracking [15]. These cuts are summarized in Tab. 3.1. The d_0 cuts can be also interpreted as follows:

$$\begin{array}{lcl} d_0 < 500 \text{ mm} & \Rightarrow & \text{all TRT layers and at least one SCT layer} \\ d_0 < 250 \text{ mm} & \Rightarrow & \text{all SCT layers} \\ d_0 < 40 \text{ mm} & \Rightarrow & \text{all Pixel layers} \end{array}$$

It seems to be interesting to look on the impact of these cuts to a number of particles passing through and their angular distribution. As expected, the number of track decreases if a tighter cut is used, but what about the distribution? Comparisons of η and ϕ distributions between four different cuts are shown on the Fig. 3.5. The normalized distributions are very similar except for cut *tight* (probably because of the low statistics) and the peak at $\eta = 0$ in the cut *loose* (because of an ***or*** between silicon and TRT hits). Numbers of particles passing through are summarized in Tab. 3.2. The *medium* cut seems to be optimal, so I have chosen it for my further research.

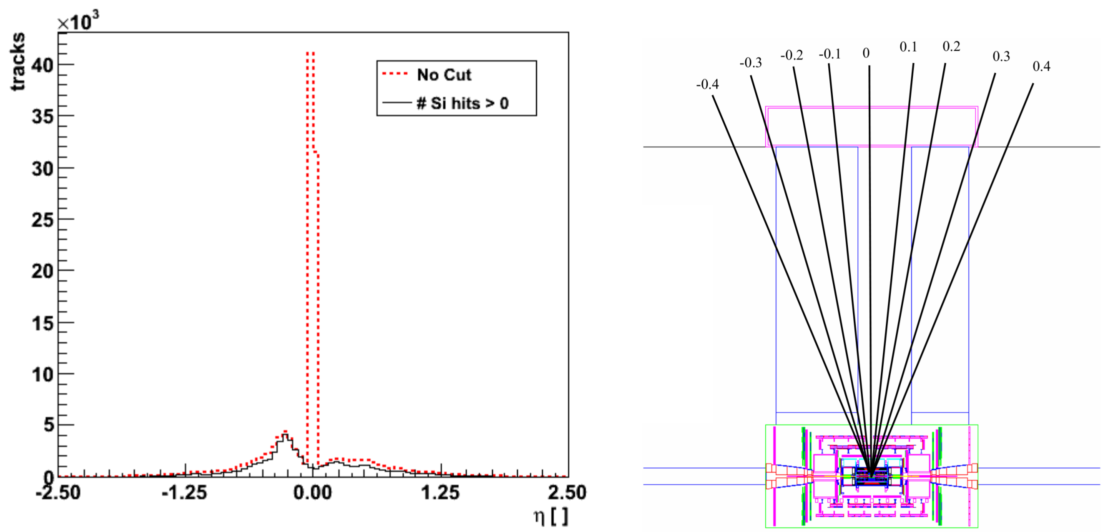

Figure 3.4: The algorithm is also able to reconstruct track form TRT hits only, but the information about η and z_0 are completely lost in this case: as you can see on right picture (the y-z view on the ATLAS cavern with access shafts; figure from [25]), there cannot be such peak at $\eta = 0$ (on the left histogram), because of all the material above the ATLAS cavern. The main maximum can be expected at $\eta \to -0.2$, the second one at $\eta \to 0.3$. That corresponds to the black solid line (of the left histogram), which represents the cut "*at-least-one-silicon-hit*". However, using this cut we lose more than 60 % of tracks. Fortunately, this should not happen in the case of tracking the collisions products.

Cut Type	Number of Hits				d_0 [mm]	p_T [GeV]
	Pixel	SCT	Silicon	TRT		
Loose	-	-	$\geq$ 8	≥ 30	< 500	> 1
Medium	-	-	≥ 10	≥ 20	< 250	> 1
Tight	≥ 4	≥ 12	-	≥ 50	$<$ 40	> 1

Table 3.1: Three agreed sets of cuts, which will be compared in further histograms. The number of hits cuts solely refer to barrel hits. The *loose* cut for silicon and TRT hits is an ***or*** requirement - the track should have either at least 8 silicon hits ***or*** at least 30 TRT hits. Table from [15].

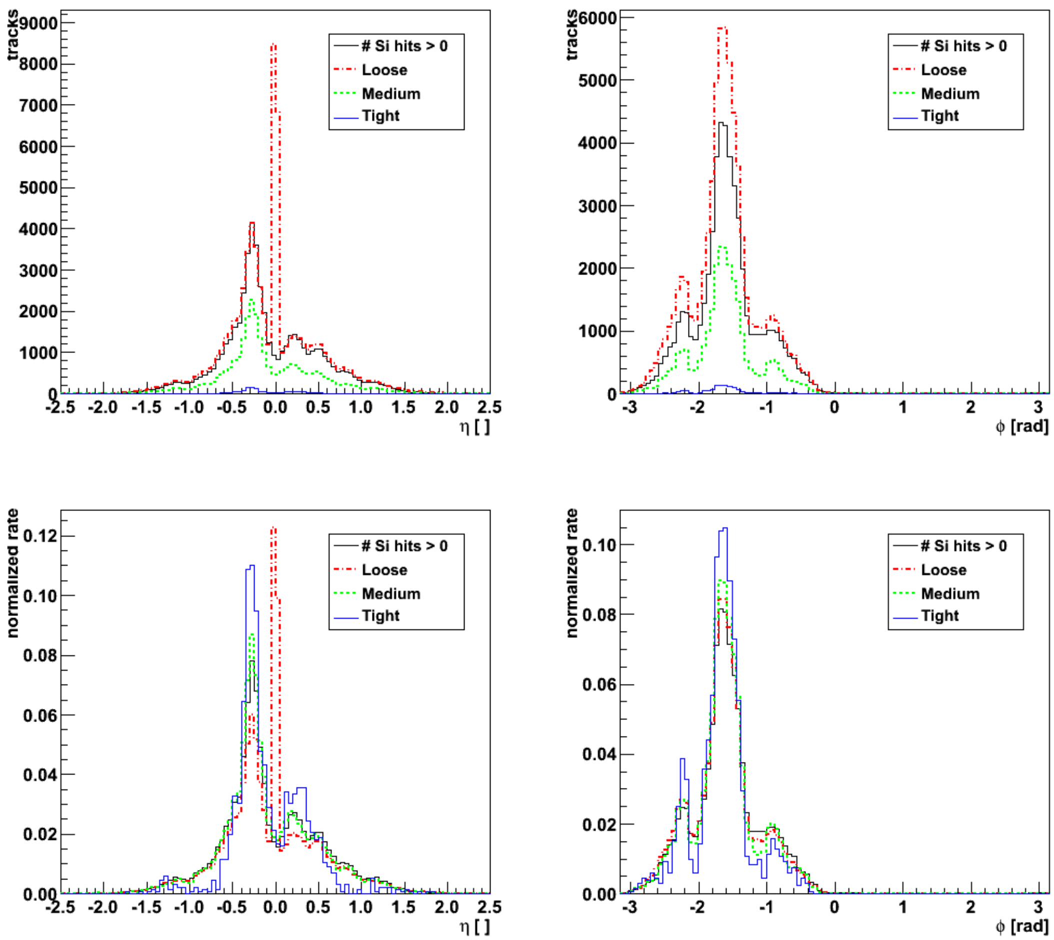

Figure 3.5: Comparisons between four different cuts in terms of track parameters η and ϕ (bottom histograms are normalized). On the top left plot you can see that the cut *at-least-one-silicon-hit* is nearly the same as the cut *loose*, except the peak on $\eta = 0$. That is the same case as on the Fig. 3.4. Because of this I think the cut *loose* is absolutely insufficient for cosmic studies.

	Cut Type	InDet Tracks	InDet %	Combined Tracks	Combined %
Real Data	No Cut	136977	100.0	51242	100.0
	# Si hits > 0	52993	38.7	45655	89.1
	Loose	69041	50.4	46359	90.5
	Medium	**26051**	**19.0**	**22969**	**44.8**
	Tight	1317	1.0	1159	2.3
MC	No Cut	150127	100.0	59024	100.0
	Medium	**19093**	**12.7**	**18320**	**31.0**

Table 3.2: Numbers of cosmic muons tracks for five different cuts. For further research I have chosen the cut *medium* (see Tab. 3.1).

Having the final cut, I could make some comparisons between real and simulated data and also have a short look at the properties of measured cosmic rays. On the Fig. 3.6 you can see a distribution of muon momentum measured by the Inner Detector. An apparent difference is between maximums of real and simulated distributions, however from 10 GeV there is very good agreement. I am not sure the cause of this - as you can see in the Tab. 3.2, the statistics are nearly the same.

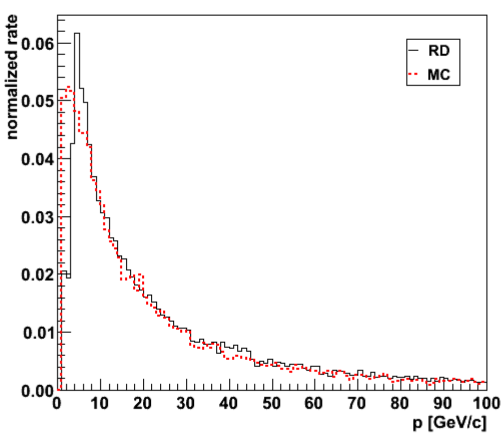

Figure 3.6: The distribution of cosmic muons momentum measured by the Inner Detector. Black solid line - real data, red dashed line - simulated data.

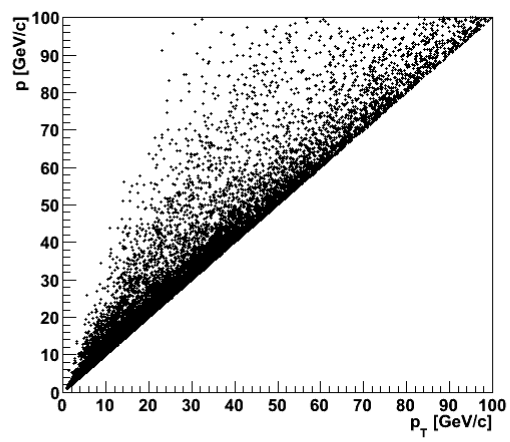

Figure 3.7: The correlation between p and p_T of cosmic muons (measured by the Inner Detector). As one can expect p_T approaches p for most of them.

What is also interesting is the ratio between positively and negatively charged muons. As you can see on the Fig. 3.8, in the range $\langle 0; 100 \rangle$ GeV/c the ratio between positively and negatively charged muons should be approximately 1.25, but real data (RD) and simulated data (MC) from the ATLAS detector show something different (see Fig. 3.9): with no cut, the ratio is 1.40 for RD and 1.34 for MC and using the *medium* cut, the ratio is 1.51 for RD and 1.54 for MC. Again, for that I do not have any explanation, but I am still working on it. The similar problem is with the ϕ distribution. While the shape of the η distribution looks as expected, not so the ϕ distribution: distributions of μ^+ and μ^- should be the same, just turned around $\phi = -\frac{\pi}{2}$ (because of the ATLAS symmetry across y-z plane and because of the histogram normalization). However as you can see on the Fig. 3.10 (right), the distribution of μ^+ has a higher main peak.

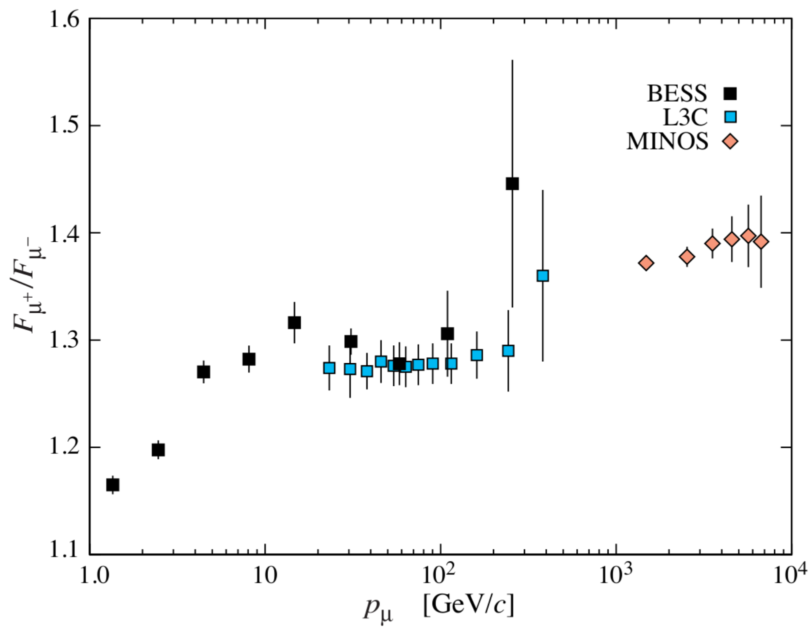

Figure 3.8: Muon charge ratio as a function of the muon momentum. These data have been measured by other experiments. Figure from [1].

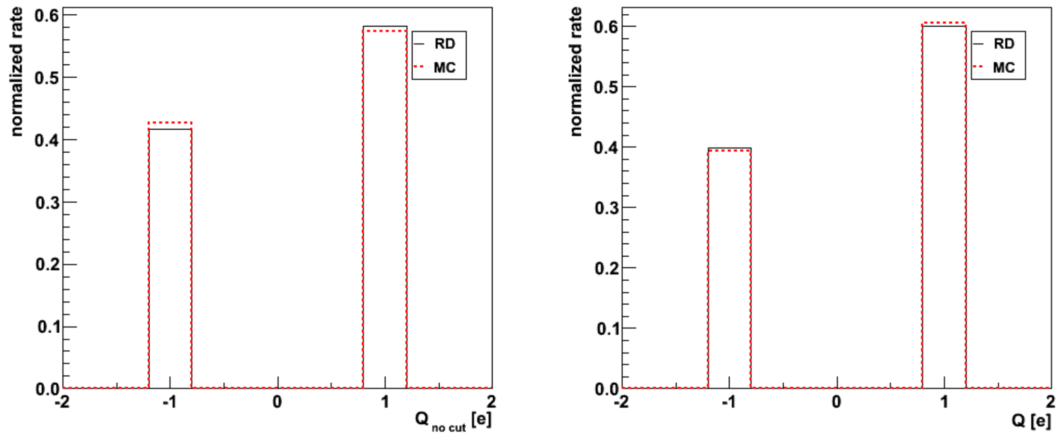

Figure 3.9: Ratios between μ^+ and μ^- and comparisons between real data (RD, black solid line) and MC simulation (red dashed line). For the left histogram no cut were used, for the right one the cut *medium* were used. Ratio should be approximately 1.25, but these histograms show something different: with no cut, the ratio is 1.40 for RD and 1.34 for MC and using the *medium* cut, the ratio is 1.51 for RD and 1.54 for MC.

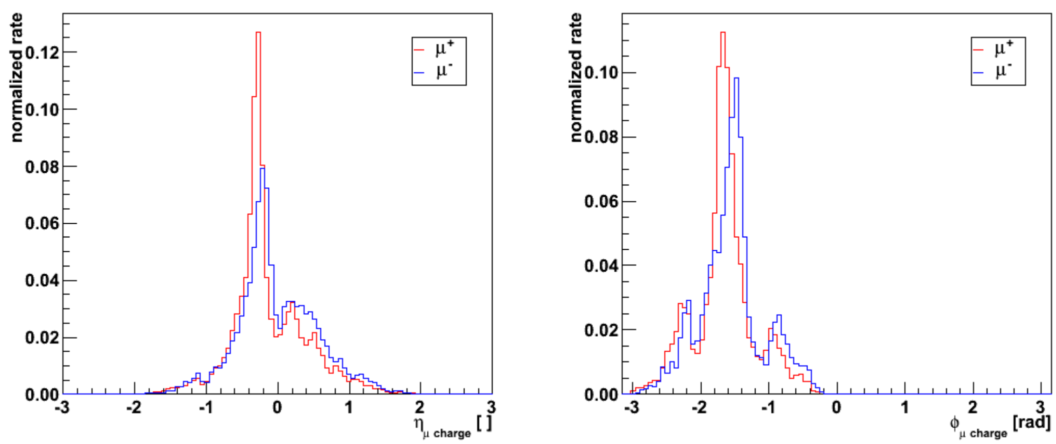

Figure 3.10: The comparison between distributions of μ^+ and μ^- in terms of η and ϕ. Data were taken with toroidal and solenoidal magnetic fields *ON*. The toroidal field affects an η of tracks, the solenoidal field affects an angle ϕ. While the shape of the η distribution looks as expected, not so the ϕ distribution: distributions of μ^+ and μ^- should be the same, just turned around $\phi = -\frac{\pi}{2}$ (because of the ATLAS symmetry across y-z plane and because of the histogram normalization). However, the distribution of μ^+ has a higher main peak. (On these plots, the effect of four access shafts is clearly visible.)

The second thing of my interest were combined studies - the alignment between the Inner Detector and the Muon Spectrometer. Track parameters from the Muon Spectrometer were extrapolated to the beam axis and then compared with the Inner Detector track parameters. For these studies, no global ID-MS alignment corrections were applied. On the Fig. 3.11 you can see correlations between ID and MS track parameters θ and ϕ. To obtain these plots I used the cut *medium*.

Also in this part I compared real and simulated data. These comparisons are shown on the Fig. 3.12. The Inner Detector and the Muon Spectrometer are well aligned, but not as well as the simulation has predicted. Thus some corrections have to be implemented into the ATLAS geometry description.

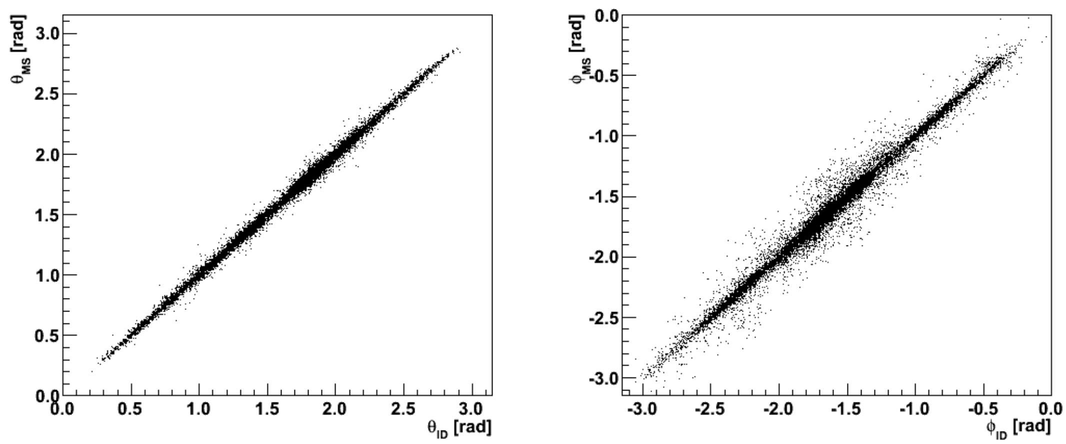

Figure 3.11: Correlations between Inner Detector (ID) and Muon Spectrometer (MS) track parameters θ and ϕ. The cut *medium* was used. The ϕ correlation would be better if the cut "*at-least-one-RPCϕ-hit*" was used, but this would also lower the statistic and reduce the range of the angle θ (about 0.3 rad on each side).

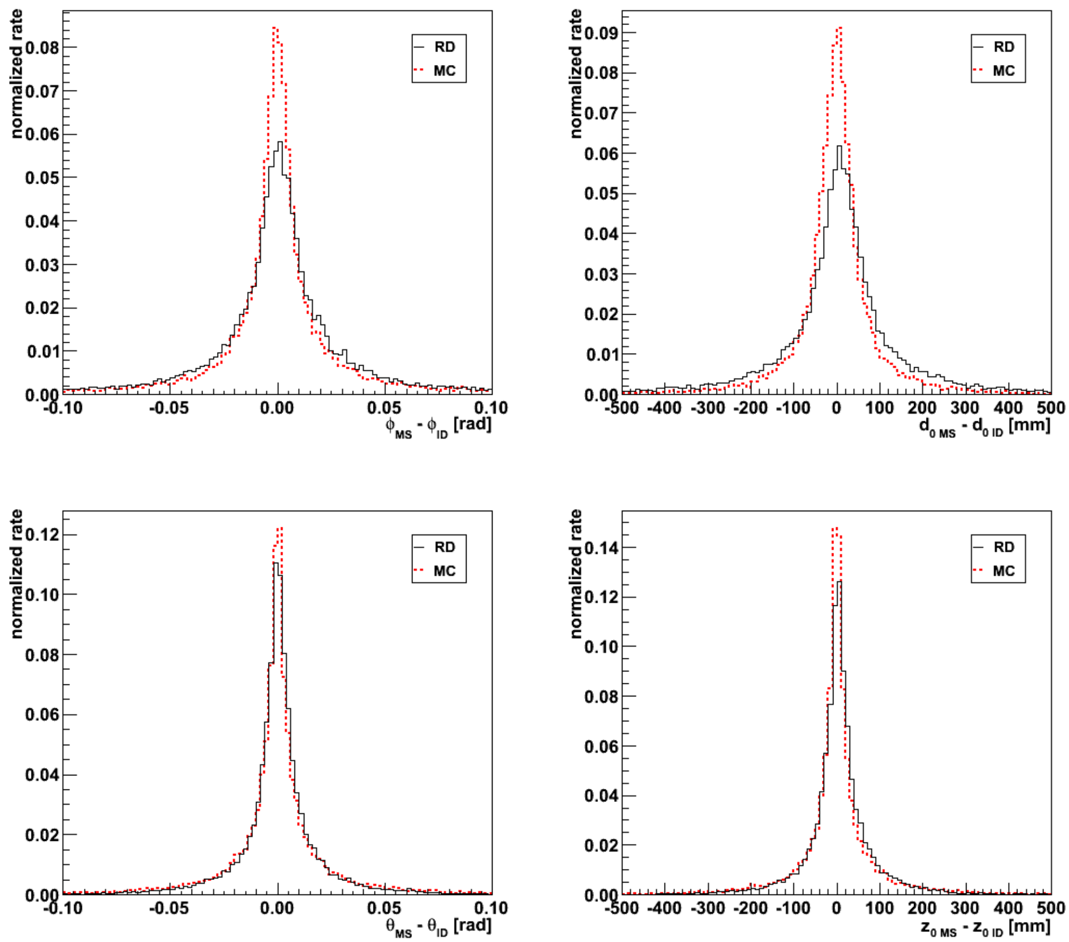

Figure 3.12: Differences between Inner Detector (ID) and Muon Spectrometer (MS) track reconstruction in terms of basic tracks parameters. Comparisons between real (black solid line) and simulated (red dashed line) data are shown. Both subdetectors are well aligned, but not as well as the simulation has predicted (mainly ϕ and d_0).

Chapter 4

Conclusions

My research was aimed at using cosmic muons for the evaluation of the ATLAS Inner Detector. I have done this research using the combined run 91890 (relatively high statistics, complete Inner Detector and Muon Spectrometer, both magnetic fields *ON*) and the equivalent sample of simulated data. I was interested in the Inner Detector tracking and also in the differences between track properties measured by the Inner Detector and by the Muon Spectrometer.

Because of the Inner Detector design and the tracking algorithm (which can make a track only from TRT hits), it is necessary to make a set of cuts for cosmic tracking. There are three agreed sets: *loose*, *medium* and *tight*, see Tab. 3.1. On the basis of the histograms on the Fig. 3.5 and data in the Tab. 3.2, I have chosen the cut *medium* as the best one for cosmic studies.

As one can see on the Fig. 3.11 and 3.12, the correlation of track parameters between the Inner Detector and the Muon Spectrometer is fairly good (using the cut *medium*), but not as good as the simulation has predicted (mainly ϕ and d_0).

I have also made some comparisons between positively and negatively charged muons. According to [1], the ratio μ^+/μ^- should be approximately 1.25, but real data (RD) and simulated data (MC) from the ATLAS detector show something different: with no cut, the ratio for RD (MC) is 1.40 (1.34) and using the *medium* cut, the ratio is 1.51 (1.54). The ϕ distribution (see the Fig. 3.10) has similar feature. This fact merits more attention, thus it will probably be one of the tasks for my further research.

Bibliography

[1] W. - M. Yao *et al.* (Particle Data Group), J. Phys. G 33, 1 (2006) and 2007 partial update for the 2008 edition available on the PDG web pages: `http://pdg.lbl.gov/`

[2] D. Rainwater, *Searching for the Higgs boson*, hep-ph/0702124v1

[3] D. H. Perkins, *Introduction to High Energy Physics*, Cambridge University Press, UK, 2000

[4] J. H. Schwarz, *The Second Superstring Revolution*, `http://www.theory.caltech.edu/people/jhs/strings/index.html`

[5] LHC machine outreach, `http://lhc-machine-outreach.web.cern.ch/lhc-machine-outreach`

[6] CERN FAQ - LHC the guide, available from: `http://cdsweb.cern.ch/record/1092437/files/CERN-Brochure-2008-001-Eng.pdf`

[7] ATLAS experiment public pages, `http://atlas.ch`

[8] HyperPhysics - Cosmic Rays, `http://hyperphysics.phy-astr.gsu.edu/Hbase/astro/cosmic.html#c2`

[9] Ultra High Energy Cosmic Rays (UHECR), `http://www.physics.adelaide.edu.au/astrophysics/hires/uhecr.html`

[10] ATLAS HLT/DAQ/DCS Group, *ATLAS High-Level Trigger, Data Acquisition and Controls Technical Design Report*, CERN, 2003, available from: `http://cdsweb.cern.ch/record/616089/files/cer-002375189.pdf`

[11] S. Fratina *et al.*, *The TRT Fast-OR Trigger* (Draft), CERN, 2009, available from: `http://cdsweb.cern.ch/record/1198833/files/ATL-COM-INDET-2009-042.pdf`

[12] ATLAS Twiki pages - InDet Tracking Performance Plots from the CSC Book, https://twiki.cern.ch/twiki/bin/view/Atlas/InDetTrackingPerformanceCSCFigures

[13] ATLAS Collaboration, *Expected Performance of the ATLAS Experiment: Detector, Trigger and Physics*, CERN, 2008, available from: http://cdsweb.cern.ch/record/1125884/files/CERN-OPEN-2008-020.pdf

[14] T. Cornelissen, M. J. Costa, M. Moreno Llácer, *Cosmic Muon Combined plots for approval*, CERN, 2009, available from: http://cdsweb.cern.ch/record/1163697/files/ATL-COM-PHYS-2009-074.pdf

[15] ATLAS Twiki pages - Analysis of Inner Detector Cosmic-Ray Data 2008, https://twiki.cern.ch/twiki/bin/view/Atlas/InDetCosmic08Analyses

[16] ATLAS Twiki pages - Trk::Perigee Class Reference, http://atlas-computing.web.cern.ch/atlas-computing/links/nightlyDevDirectory/AtlasOffline/latest_doxygen/InstallArea/doc//TrkParameters/html//classTrk_1_1Perigee.html

[17] NYU participation in ATLAS, http://www.physics.nyu.edu/experimentalparticle/atlas.html

[18] V. Lacuesta, *Alignment of the Atlas Inner Detector tracking system*, TIPP 2009, available from: https://twiki.cern.ch/twiki/pub/Atlas/AtlasIDAlignPresentations/VicenteTIPP09.pdf

[19] ATLAS Twiki pages - The ATLAS Computing Workbook, https://twiki.cern.ch/twiki/bin/view/Atlas/WorkBook

[20] ATLAS Computing Group, *ATLAS Computing Technical Design Report*, CERN, 2005, available from: http://atlas-proj-computing-tdr.web.cern.ch/atlas-proj-computing-tdr/PDF/Computing-TDR-final-July04.pdf

[21] Geant4 HomePage, http://geant4.web.cern.ch/geant4/

[22] ROOT HomePage, http://root.cern.ch/

[23] ATLAS Collaboration, *Virtual Point 1*, http://atlas-vp1.web.cern.ch/atlas-vp1/

[24] ATLAS Collaboration, *Atlantis Event Display*, http://www.hep.ucl.ac.uk/atlas/atlantis/

[25] S. Zenz, *Simulation of Cosmic Muons in the ATLAS Tile Calorimeter*, University of Chicago, available from: http://hep.uchicago.edu/atlas/tilecal/commissioning/Zenz.doc